DELPHI Collaboration DELPHI 2002-056 CONF 590
1 July, 2002

ZZ production in e^+e^- interactions at $\sqrt{s} = 183 - 209$ GeV

G. Borisov
University of Lancaster
N. Kjaer, I. van Vulpen
CERN
R. Contri
INFN Genova
J. Rehn
Inst. für Exper. Kernphysik, Karlsruhe
K. Cieslik, M. Witek
INP, Krakow (supported by KBN 2P03B11116, SPUB P03DZ297/2000)
P. Bambade
LAL, Orsay
T. Baroncelli, E. Graziani
Universita Roma 3
E. Ferrer Ribas, R. Nicolaidou
CEA, Saclay
M. E. Pol
CBPF, Rio de Janeiro
M. Begalli, LL. M. Mundin
UERJ, Rio de Janeiro

Abstract

Measurements of on-shell ZZ production are described, using data collected by the DELPHI experiment at LEP in e^+e^- collisions at centre-of-mass energies between 183 and 209 GeV, corresponding to an integrated luminosity of about 665 pb^{-1}. Results obtained in each of the final states $q\bar{q}q\bar{q}$, $\nu\bar{\nu}q\bar{q}$, $\mu^+\mu^-q\bar{q}$, $e^+e^-q\bar{q}$, $\tau^+\tau^-q\bar{q}$, $l^+l^-l^+l^-$, and $\nu\bar{\nu}l^+l^-$ are presented. The measured production cross-sections are consistent with the Standard Model expectations. These results update and supersede those already published at 183 and 189 GeV.

Contributed Paper for ICHEP 2002 (Amsterdam)

1 Introduction

The first evidence [1] for doubly resonant production of Z bosons was observed during 1997, at the beginning of the LEP-2 period of operation, when the accelerator reached a centre-of-mass energy near 183 GeV, corresponding to the threshold for this channel. In this article we present measurements of the production cross-section, using data collected by the DELPHI [2] experiment in 1997-2000, at centre-of-mass energies up to 209 GeV, corresponding to an integrated luminosity of about 665 pb^{-1}.

There are several motivations for studying this channel. Firstly, it enables to check the Standard Model (SM) prediction. Both the cross-section and angular distribution of the produced Z bosons are sensitive to contributions from new physics beyond the SM. Several mechanisms for anomalous production [3, 4] can hence be constrained directly. For instance limits on anomalous neutral-current triple gauge boson couplings [5] can be set. Secondly, the ZZ production process forms an irreducible background to the Higgs search at LEP, when the mass of the Higgs boson is close to that of the Z [6]. It provides an environment similar to that corresponding to a possible Higgs signal, in the main decay channels $b\bar{b}Z$, both in terms of experimental signature and rate. In this context the results obtained can give an indication of the reliability of the techniques used in the Higgs search.

In what follows, the data sets and simulations used are described, and the signal definition adopted is discussed. The event selections developed are presented for each of the seven sub-channels which were analysed[1]: $q\bar{q}q\bar{q}$, $\nu\bar{\nu}q\bar{q}$, $\mu^+\mu^-q\bar{q}$, $e^+e^-q\bar{q}$, $\tau^+\tau^-q\bar{q}$, $l^+l^-l^+l^-$, and $\nu\bar{\nu}l^+l^-$ (with $l = e, \mu, \tau$). Results are given in the form of a comparison of the numbers of found and predicted selected events, together with an evaluation of the main systematic effects. Finally, combinations of sub-channel results into overall ZZ cross-sections at each centre-of-mass energy are described, as well as combinations performed over all centre-of-mass energies, both separately in each sub-channel, and for all channels together. The resulting measurements are compared to SM expectations.

These results update and supersede those already published at 183 and 189 GeV[7]. Measurements of on-shell ZZ production published by the three other LEP collaborations can be found in [8, 9, 10].

2 Data samples and simulation

The centre-of-mass energies and integrated luminosities corresponding to the data samples collected by DELPHI in the years 1997-2000 are given in Table 1. A detailed description of the detector and a review of its performance can be found in [2, 11]. For LEP-2 operation, the vertex detector was upgraded [12] and a set of scintillator counters was added to veto photons in blind regions of the electromagnetic calorimetry, at polar angles $\theta \simeq 40^\circ$ and $\theta \simeq 90^\circ$.

Simulated events were produced with the DELPHI simulation program `DELSIM`[11] and were then passed through the same reconstruction and analysis chain as the data. The generation of processes leading to four-fermion final states was done with `EXCALIBUR`[13],

[1] Track selections and jet clustering algorithms used in the selections were similar, though not identical, among the different sub-channels. They are mentioned explicitly in the descriptions of the analyses only when particularly relevant.

relying on JETSET 7.4 [14] for quark fragmentation. GRC4F[15] was used as a complementary generator for four-fermion final states resulting from single-resonant $We\nu_e$ and $(Z/\gamma^*)e^+e^-$ processes when the spectator electron was close to the beam direction. Two-fermion processes $e^+e^- \rightarrow q\bar{q}(\gamma)$ were generated using PYTHIA [14], $e^+e^- \rightarrow \mu^+\mu^-(\gamma)$ and $e^+e^- \rightarrow \tau^+\tau^-(\gamma)$ with KORALZ[16], and $e^+e^- \rightarrow e^+e^-(\gamma)$ with BHWIDE[17]. Two-photon interactions were generated using TWOGAM [18] and BDK [19].

During 2000, one sector of the main tracking device TPC (1/12 of the whole detector) was inactive from the beginning of September to the end of data taking, which corresponded to about a quarter of the 2000 data sample. The corresponding small change of analysis sensitivity from this period was taken into account in the extraction of the cross-sections.

Year	$\sqrt{s}$ [GeV]	Integrated luminosity [pb^{-1}]
1997	182.6	54.0
1998	188.6	158.1
1999	191.6	25.8
1999	195.5	76.9
1999	199.5	84.3
1999	201.6	41.1
2000	< 205.5	83.3
2000	> 205.5	141.8
Total	-	665.3

Table 1: Centre-of-mass energies and integrated luminosities of the data collected by DELPHI in the years 1997-2000. During the year 2000, the energies reached were in the range 202-209 GeV, clustered mainly around 205 and 207 GeV.

3 Signal definition

The region of phase-space at high di-fermion masses which characterizes ZZ production must be isolated to measure the corresponding cross-section. In this region, besides the dominant tree-level doubly-resonant ZZ production graphs shown in Figure 1 (referred to as the NC02 graphs), there are also contributions from other four-fermion processes, which can lead to identical final states[2]. In order to interpret the measurements in terms of NC02 graphs, the ZZ signal was defined in each of the sub-channels by pre-selecting a sub-set of events within the four-fermion simulation, having both a high purity and efficiency in terms of relative contribution from the dominant NC02 graphs. In the selections of $l^+l^-q\bar{q}$ final states (with $l = e, \mu, \tau$), and in the probabilistic $\nu\bar{\nu}q\bar{q}$ selection used as cross-check (see Sections 5-7), the signal definition used was based on cuts on the generated boson masses, which were required to be within 10 GeV/c^2 of the nominal Z mass [7]. In the other sub-channels, the signal was defined as the sub-set of events satisfying:

[2]Such contributions arise from $Z\gamma^*$ and $\gamma^*\gamma^*$ processes (when γ^* virtualities are close to M_Z), from single-resonant processes $(Z/\gamma^*)e^+e^-$ (in cases of final states with electrons), and from W boson pair production (in cases of $u\bar{u}d\bar{d}$, $c\bar{c}s\bar{s}$, and $\nu_l\bar{\nu}_l l^+l^-$ final states).

$$\frac{|\mathcal{M}_{\mathrm{NC02}}|^2}{|\mathcal{M}_{\mathrm{All}}|^2} > 0.5,$$

where $\mathcal{M}_{\mathrm{NC02}}$ and $\mathcal{M}_{\mathrm{All}}$ are the matrix elements for NC02 and for all four-fermion graphs, respectively. Corrections were then necessary to relate the measured values to NC02 cross-sections[3], in order to take into account the efficiency of the signal-defining selection cut, the residual contamination from the non-NC02 processes, and interference effects. However, because NC02 and non-NC02 contributions are naturally well separated in phase-space, the magnitudes of these corrections were quite small (typically less than a few percent).

Figure 1: The Feynman graphs for on-shell ZZ production (referred to as the NC02 graphs)

4 Four jets

The $q\bar{q}q\bar{q}$ decay mode represents 48.9% of the ZZ final states. It results typically in four or more reconstructed jets of particles. The dominant backgrounds originate from fully hadronic WW final states and from $q\bar{q}(\gamma)$ processes with hard final state gluon radiation, both of which can lead to similar multi-jet topologies. The main ingredients used to isolate the signal were b-tagging of the jets, topological information quantifying jet separation and kinematics, and di-jet mass reconstruction. A probabilistic method based on likelihood ratio products was developed to combine the information and compute an event-by-event measure of the compatibility with the ZZ hypothesis.

4.1 Event pre-selection

A pre-selection was applied to select fully hadronic events. Firstly, events were required to contain at least 18 charged tracks and to have more than 80% of the available centre-of-mass energy observed in the detector. To reduce the contamination from $q\bar{q}(\gamma)$ processes with energetic photons emitted in the beam pipe, $\sqrt{s'}$ the reduced mass of the event, computed from the jet directions, was required to exceed 69% of $\sqrt{s}$. Particles were then clustered into jets using the DURHAM clustering algorithm (y_{cut}=0.001) and events were

[3]Destructive interference from Fermi correlations occurs in the case of final states with four identical fermions [20]. Although modeled by the four-fermion simulation, the resulting reductions in overall cross-section, smaller than 0.5%, were neglected in the calculation of these NC02 cross-sections.

selected if four or more well separated jets were reconstructed[4]. To reduce backgrounds from processes with energetic and isolated leptons or photons, jets were required to contain at least four particles and have an invariant mass above 1 GeV/c^2. Four and five jet events were treated separately throughout the analysis. The efficiency of these cuts was about 88% and 80% for the fully hadronic ZZ signal and WW background, respectively, while only 2% of $q\bar{q}(\gamma)$ processes remained. At this stage, backgrounds from all other processes were negligible.

4.2 Probabilistic selection

A method based on likelihood ratio products was developed to compute the relative probabilities for any given pre-selected event to originate from one of the three SM processes, WW, ZZ and $q\bar{q}(\gamma)$. The three main features used to isolate the ZZ signal from the background processes were the presence of B-hadrons in the jets, the reconstructed di-jet masses, and the jet kinematics and separation. The computation combined measurements of the events with the theoretical expectations corresponding to each hypotheses (described analytically where possible).

B-hadrons in the jets were identified using a dedicated algorithm [21] which exploited their characteristically longer lifetime and larger mass. This was made possible by the capabilities of the vertex detector [12], in which tracks originating from the displaced B-hadron vertices could be resolved. The combined b-tagging variable which was constructed is shown in Figure 2 for jets in hadronic Z decays (left plot), and in the pre-selected fully hadronic high-energy event sample (right plot). The combined b-tagging variable was particularly powerful to reduce the contamination from WW events, since the corresponding final states hardly ever contain a b-quark, while 38.7% of fully hadronic ZZ events have at least two b-quarks. In order to optimally use the information, the ratio of the distributions of this variable for jets originating from the fragmentation of b and non-b quarks was parameterised in three different angular regions, using simulated Z decays, to take into account the polar angle dependence of the detector resolution. Using these parameterisations and the values measured for each jet, relative b and non-b probabilities could be assigned to each jet.

Reconstructed mass distributions can also be used to characterise the different hypotheses. The expected mass distributions are well defined. But experimentally there are some difficulties, since in a four or five-jet event, there are three or ten possible jet-jet pairings, respectively. In addition, the quality of the energy flow reconstruction can vary significantly from event to event. These considerations were taken into account by evaluating simultaneously the compatibility of each of the possible jet-jet pairings with each hypothesis considered, WW, ZZ and $q\bar{q}(\gamma)$. For this purpose, the expected probability distributions for the different mass combinations in an event were first expressed in analytical form, as products of Breit-Wigner distributions and phase-space factors for the correctly paired mass combinations in WW and ZZ events, and as flat spectra for all other cases. Experimentally, the errors on the four-momenta of the jets were then used for each event in kinematic fits [22] requiring four-momentum conservation and equality of each di-jet mass with pairs of values to be tested. The two-dimensional χ^2 probability distributions obtained from these fits as a function of the test values were then folded

[4]Events with six or more reconstructed jets were forced into a five-jet configuration.

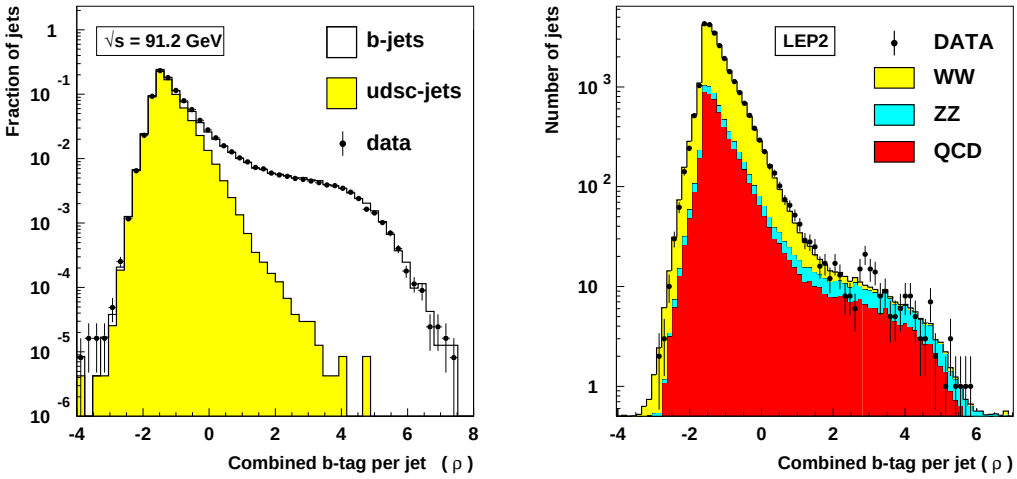

Figure 2: The left plot shows the combined b-tag variable for jets in Z-decays. The right plot shows the combined b-tag probability per jet for all reconstructed jets after the pre-selection in the full LEP-2 data-sample. The dots are the data and the histograms represent the simulation.

with the expected probability distributions to quantify the compatibility of each pairing with the WW, ZZ and $q\bar{q}(\gamma)$ hypotheses, from the mass information alone. As an illustration, the distribution of the WW-compatibility, obtained by combining all jet-pairings, is shown in the left plot of Figure 3 (for the pre-selected events which were clustered into four jets). The main advantage of this method was that the inherent ambiguity in the pairing of the jets, the main difficulty in the experimental analysis of multi-jet events, did not need to be resolved, each possible pairing being assigned a probability.

Finally, specific features of the jet kinematics and separation in events arising from four-fermion and $q\bar{q}(\gamma)$ processes with hard final state gluon radiation leading to a four-jet event were exploited. Because gluon emission off quarks has infrared and collinear divergences, the latter tend to have cigar-like shapes, while the four-fermion processes are more spherical. This difference was used to construct a topological variable: $\mathrm{D_{pur}} = E_1\theta_1\sqrt{E_2\theta_2}/10$, where E_1 (E_2) is the leading (subleading) jet energy and θ_1 (θ_2) is the smallest (one but smallest) opening angle between two jets. The ratio of these two event types was parameterised as a function of this variable using simulated data, for four and five jet events separately. The distribution of the $\mathrm{D_{pur}}$ variable for four-jet events is shown in the right plot of Figure 3.

Considering all possible hadronic ZZ final states and using the predicted SM cross-sections and branching ratios into the different quark configurations, the probability of jets to originate from b-quarks, the topological information per event and the mass information per pairing, a combined variable quantifying the compatibility of each event with the ZZ hypothesis was constructed. Its distribution is shown in Figure 4, including the data from all centre-of-mass energies. It was shown to behave as a genuine probability; the distribution of the purity of ZZ events with respect to the constructed variable being identical for all energies, the different energies could be added without diluting the information.

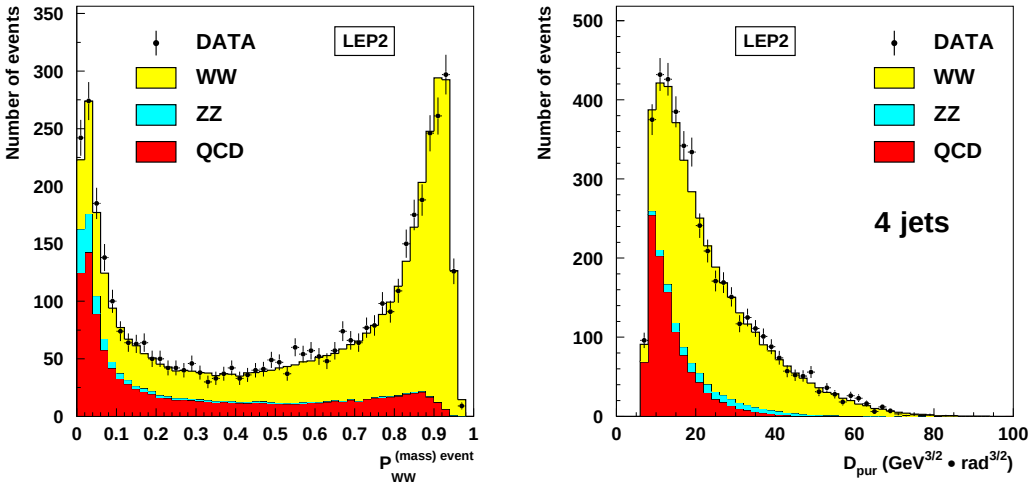

Figure 3: The left plot shows for each event the (normalised) compatibility with a WW hypothesis, computed using only mass information. The right plot shows the event-topology variable D_{pur}. Both distributions are for pre-selected events which were clustered into four jets (corresponding to about 80% of the total sample). The dots are the data taken in 1997-2000 and the histograms represent the simulation.

4.3 Results

The observed and predicted numbers of events selected after cuts on the ZZ probability maximising the products of efficiency and purity are shown in Table 2. There was an overall agreement between data and simulation within the statistical fluctuations. At each centre-of-mass energy, a measurement of the production cross-section was obtained from a binned maximum likelihood fit to the distributions of the ZZ probability, with the ZZ signal contribution as the only free parameter. The results obtained and the combinations performed with other channels to derive global values for the NC02 cross-section are described in Section 10. The optimal region of the ZZ probability distribution to be used in the fit was determined by minimising the combined statistical and systematic uncertainty, evaluated using the full LEP-2 data sample. This procedure resulted in excluding from the fitting events with a ZZ probability lower than 0.25. At this level, the contributions from the WW, $q\bar{q}(\gamma)$ and ZZ events were comparable.

4.4 Systematic uncertainties

The main source of systematic error in the selection of $ZZ \to q\bar{q}q\bar{q}$ events was from the limited precision available in the modelling of the multi-jet $q\bar{q}(\gamma)$ processes (particularly those involving b-quarks) which composed the main background in the most signal-like regions relevant to the extraction of ZZ cross-sections. Theoretical uncertainties in the predictions and biases from the generator treatments were studied at $\sqrt{s} = M_Z$ and extrapolated to LEP-2 energies [23]. The most relevant aspects for the measurement of the $q\bar{q}q\bar{q}$ channel are summarised below.

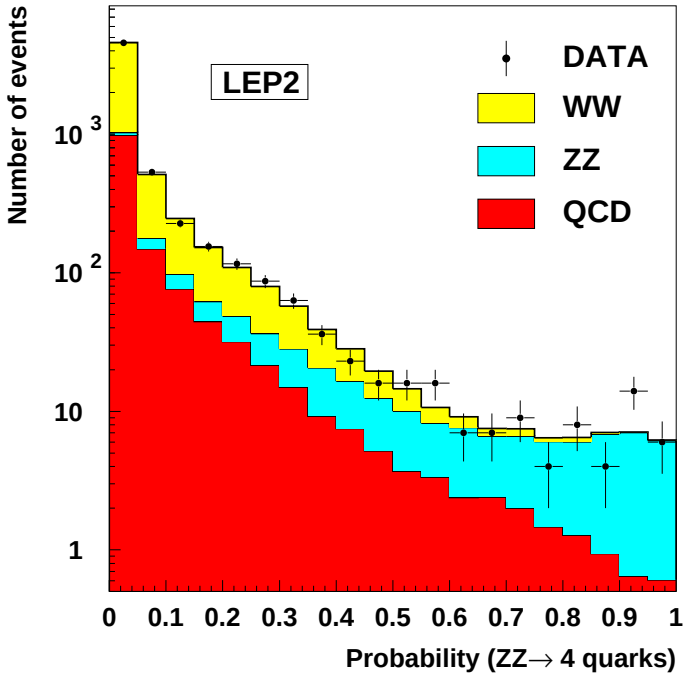

Figure 4: Distribution of the combined ZZ probability. The dots are the data taken in 1997-2000 and the histograms represent the simulation.

It was found that PYTHIA underestimated the inclusive four-jet rate[5] by typically 10% at $\sqrt{s} = M_Z$. This discrepancy was confirmed by comparisons at LEP-2 energies, and was used as a conservative estimate of the corresponding uncertainty, treating the resulting error as one-sided.

The probability of secondary c and b-quark pair production through gluon splitting processes was found to be underestimated in PYTHIA by factors of about 1.5 and 2, respectively, compared to other calculations and dedicated measurements. An approximate correction of this deficit was achieved in the analysis by reweighting simulated events containing gluons splitting into heavy quarks with these factors. Since the gluon splitting process remains poorly known both theoretically and experimentally, and since the reweighting procedure applied provided only a rough correction, a $\pm$ 50% relative error on these probabilities was assumed.

The magnitude of the reduction in gluon radiation off b-quarks relative to other flavours (arising from their heavier mass) was shown to be overestimated in the version of PYTHIA used, compared to analytic calculations and to dedicated measurements, typically by as much as the theoretical uncertainty in these calculations. A $\pm$ 4% relative error in the four-jet rate from $q\bar{q}(\gamma)$ processes was conservatively assumed to cover both the uncertainty and the bias.

The impact of propagating these uncertainties in the background level to the fitted $ZZ \to q\bar{q}q\bar{q}$ cross-sections is shown in Table 3, using the full LEP-2 data sample. The

[5]The agreement between data and simulation for general hadronic event properties and shapes depends on the strategy applied in the tuning of the generator parameters[24].

$ZZ \to q\bar{q}q\bar{q}$					
$\sqrt{s}$ [GeV]	Integrated luminosity [pb^{-1}]	Selection efficiency	Predicted background	Predicted total MC	Selected data
183	54.0	0.22	3.05	4.57	2
189	158.1	0.27	17.88	31.13	29
192	25.8	0.46	11.03	15.53	20
196	76.9	0.35	16.64	28.50	39
200	84.3	0.47	42.21	61.05	55
202	41.1	0.46	17.14	26.24	30
205	83.3	0.37	19.12	33.49	35
207	141.8	0.36	33.09	59.75	54
Total	665.3	0.38	166.18	268.11	273

Table 2: Integrated luminosities, selection efficiencies and number of observed and expected events, after selections on the probability of the ZZ hypothesis maximising the product of efficiency and purity.

effect from uncertainties in selection efficiencies related to the b-tagging procedure is also shown, as well as the effect from varying the WW cross-section within ± 2% [20]. The estimate of the error from b-tagging was obtained by propagating to the computed b and non-b jet probabilities the errors evaluated in [25]. All errors were assumed to be correlated between the centre-of-mass energies analysed.

$\sqrt{s}$ [GeV]	Inclusive four-jet rate	Gluon splitting into heavy quarks	Gluon radiation off b-quarks	b-tagging procedure	WW cross-sections
183 - 208	± 2.3 %	± 2.3 %	± 1.8 %	± 1.5 %	± 0.9 %

Table 3: Expected effects on the fitted $ZZ \to q\bar{q}q\bar{q}$ cross-section from uncertainties in the predicted background and selection efficiencies.

5 Jets and missing energy

The $\nu\bar{\nu}q\bar{q}$ decay mode represents 28.0% of the ZZ final states. The event topology is characterised by a pair of jets acoplanar with the beam and with visible and recoil masses compatible with the Z mass. Because two energetic neutrinos escape detection in this channel, efficient and reliable energy flow reconstruction is essential to select the signal. The most difficult physical backgrounds arise from single-resonant $We\nu_e$ processes, from WW processes where one W decays into $\tau\nu_\tau$, and from $q\bar{q}$ events, accompanied or not by isolated photons escaping detection, in which one or both jets are badly reconstructed.

After first applying a common pre-selection to remove the bulk of the background, two independent analyses were carried out. Each analysis stream used a separate selection of discriminating variables, and combined them to construct an optimal estimator, using

two different schemes: a non-linear Fischer discriminant method (the so-called Iterative Discriminant Analysis (IDA) [26]), and a probabilistic method based on likelihood ratio products. Results from both analyses were obtained and compared. The IDA analysis was chosen to derive the combined values of the NC02 cross-section described in Section 10, and was used to study the propagation of systematic uncertainties. The probabilistic analysis served as cross-check.

5.1 Particle selection

Charged particles were selected if their momentum was greater than 100 MeV/c^2 and if they originated from the interaction region within 4 cm in the transverse plane, and within 4 cm/sin θ along the beam axis (where θ is the polar angle of the particle). Neutral particles were defined either as energy clusters in the calorimeters not associated to charged particle tracks, or as reconstructed vertices of photon conversions, interactions of neutral hadrons or decays of neutral particles in the tracking volume. All neutral clusters of energy greater than 300 MeV in the barrel electromagnetic calorimeter (HPC) and the very forward calorimeter (STIC), or 400 MeV in the forward electromagnetic calorimeter (FEMC) were used.

5.2 Event pre-selection

Events due to particles of the beam with momenta far from the nominal values were first excluded by requiring at least two charged particles with impact parameter less than 1 mm in the transverse plane and less than 3 mm along the beam axis, and with a transverse momentum greater than 2 GeV/c. A loose hadronic pre-selection was then applied, requiring at least eight charged particles, a total charged energy greater than $0.16\sqrt{s}$, a transverse energy greater than $0.15\sqrt{s}$, and the sum of all particle momenta along the thrust axis to be greater than $0.25\sqrt{s}$. Finally, events with an electromagnetic shower exceeding $0.45\sqrt{s}$ were rejected. This removed about 97% of the background from $\gamma\gamma$ and Bhabha processes.

To reject events coming from $q\bar{q}(\gamma)$ processes with energetic photons emitted in the beam pipe, $\sqrt{s'}$ the reduced mass of the event, computed from the jet directions[6], was required to be greater than 115 GeV when the polar angle of the total momentum was less than 40°. To reduce the contamination from $q\bar{q}(\gamma)$ processes with energetic photons in the detector acceptance, events were rejected if their total electromagnetic energy within 30° of the beam axis was greater than $0.16\sqrt{s}$, or if the total energy in the luminosity monitor was greater than $0.08\sqrt{s}$. To reject $q\bar{q}(\gamma)$ processes with energetic photons emitted in blind regions of the electromagnetic calorimetry (at polar angles $\theta \simeq 40°$ and $\theta \simeq 90°$) signals from a set of dedicated scintillator counters were used. To reduce the two-fermion background outside the radiative return peak as well as four-fermion backgrounds without missing energy, the reduced mass of the event had to satisfy $\sqrt{s'} < 0.96\sqrt{s}$. To reduce backgrounds from two-fermion events with jets pointing to the insensitive regions of the electromagnetic calorimeters, where the energy flow was less precise, events were rejected if the jets had polar angles within the ranges $35-45°$ or $135-145°$, unless the acoplanarity of the event was greater than 10°. This removed about 88% of the total $q\bar{q}(\gamma)$ background.

[6]Throughout this section, unless otherwise specified, the particles of the events were clustered into precisely two jets.

The contamination from WW processes where one W decayed leptonically was reduced by requiring that the energy of the most energetic particle of the event be less than $0.2\sqrt{s}$. To improve the rejection when the W decayed into $\tau\nu_\tau$, the events were required to have no charged particle with a transverse momentum with respect to its jet direction greater than 10 GeV/c. This removed about 66% of the WW background.

At the end of the event pre-selection, the efficiency for the $ZZ \to \nu\bar{\nu}q\bar{q}$ signal was about 77%.

5.3 IDA selection

After the pre-selection described in Section 5.2, it was additionally required that the momentum of the most isolated particle in the event be in the range $0.01\sqrt{s} < p < 0.20\sqrt{s}$, and that the reconstructed visible mass be smaller than $\sqrt{s}$. A combined discriminant variable was then constructed using the Iterative Discriminant Analysis program (IDA) [26] to calculate a second order polynomial from twelve event variables, selected according to their discriminating power and independence[7]:

- The logarithm of the transverse momentum to the beam axis (see Figure 5 upper left),
- The visible energy normalised to $\sqrt{s}$, for values lower than 1 (see Figure 5 upper right),
- The transverse energy normalised to $\sqrt{s}$, for values in the range $0.15 - 0.60$,
- The minimum polar angle defining a cone in the positive and negative beam directions containing 6% of the total visible energy,
- The difference of the jet energies normalised to $\sqrt{s}$, for values lower than 0.35,
- The sum of particle energies in a cone of 5° around the most isolated particle, normalised to $\sqrt{s}$, for values lower than 0.15,
- The reduced mass $\sqrt{s'}$,
- The logarithm of the product of the acoplanarity and the inter-jet angle, for values lower than 2.80 (see Figure 5 lower left),
- The logarithm of the acollinearity,
- The longitudinal momentum with respect to the thrust axis, normalised to $\sqrt{s}$, for values lower than 1,
- The missing mass normalised to $\sqrt{s}$, computed with the constraint that the visible mass equal M_Z (see Figure 5 lower right),
- The logarithm of the largest transverse momentum of any particle with respect to its jet direction.

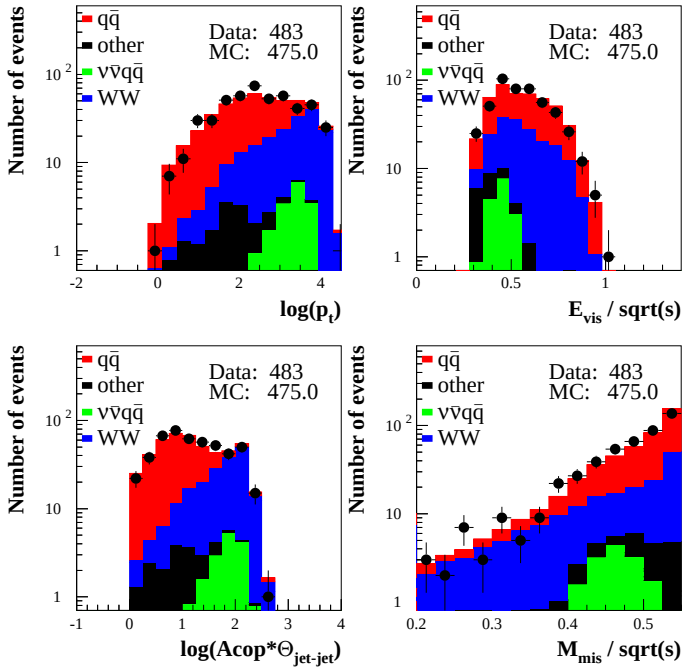

Figure 5: Logarithm of the transverse momentum with respect to the beam axis (upper left); Ratio between the visible energy and the centre-of-mass energy (upper right); Logarithm of the product of the acoplanarity and the inter-jet angle (lower left); Ratio between the missing mass (computed using the constraint that the visible mass be compatible with M_Z) and the centre-of-mass energy (lower right). These variables were used as part of the IDA analysis stream. The dots are the data taken in 1999 at a centre-of-mass energy $\sqrt{s} = 199.5$ GeV. The histograms are the simulation prediction.

The observed distributions of these twelve variables were in good agreement with the predictions from simulation, at each centre-of-mass energy analysed. As an illustration, the distributions of four among them are shown in Figure 5, for $\sqrt{s} = 199.5$ GeV. The IDA method for variable combination was applied in two successive optimisations. Following the first one, an enriched sub-sample of events was selected, with a 95% relative signal efficiency. These events were then used in the second optimisation. The final combined discriminant variable obtained is shown in Figure 6, including the data from all energies[8].

5.4 Probabilistic selection

After the pre-selection described in Section 5.2, it was additionally required that the total visible energy be lower than $0.70\sqrt{s}$. A probabilistic method based on likelihood ratio

[7]To concentrate on the signal region when optimizing the second-order discriminant function, and to avoid long non-gaussian tails, very loose cuts were applied to some of the variables, as indicated.

[8]The distribution of the purity of ZZ events as a function of the final discriminant variable was almost identical for all centre-of-mass energies, allowing to add the histograms of the different energies with minimal dilution of the information.

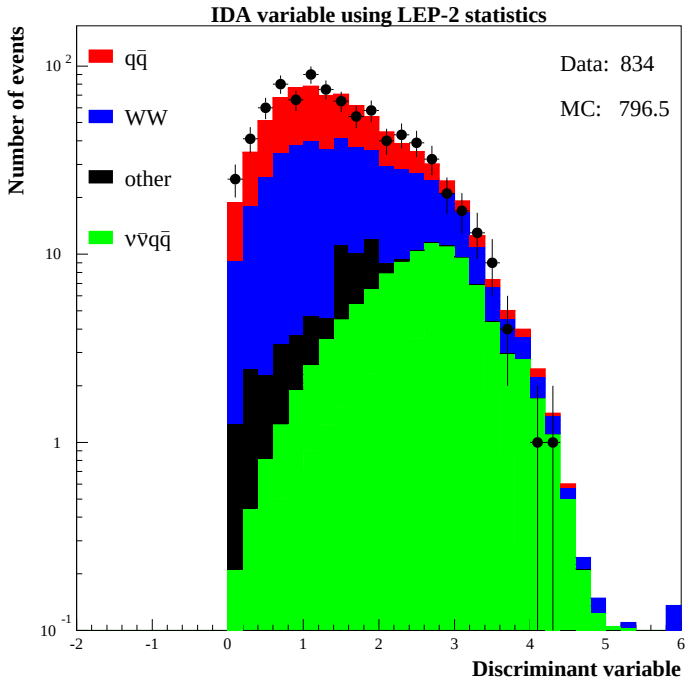

Figure 6: Combined discriminating variable for the $\nu\bar{\nu}q\bar{q}$ analysis (IDA selection). The dots are the data taken in 1997-2000 and the histograms represent the simulation.

products was then used to combine nine discriminating variables:

- The energy of the most energetic jet,
- The cosine of the acoplanarity,
- The reduced mass $\sqrt{s'}$ normalised to $\sqrt{s}$,
- The missing momentum,
- The cosine of the polar angle of the missing momentum,
- The largest transverse momentum of any particle with respect to its jet direction,
- The minimum charged multiplicity of the jets, defined in this case by clustering the particles of the events without requiring precisely two jets,
- The visible mass, computed with the constraint that the missing mass equal M_Z,
- The output of a veto algorithm based on the response of the dedicated scintillator counters installed at at polar angles $\theta \simeq 40°$ and $\theta \simeq 90°$.

There was a good agreement between the data and the predictions from the simulation for each of these variables, at each centre-of-mass energy. The probability density functions used to construct the combined discriminant variable were determined from the simulation, separately at each energy. The distribution of this final variable is shown in Figure 7 for the data collected in 2000.

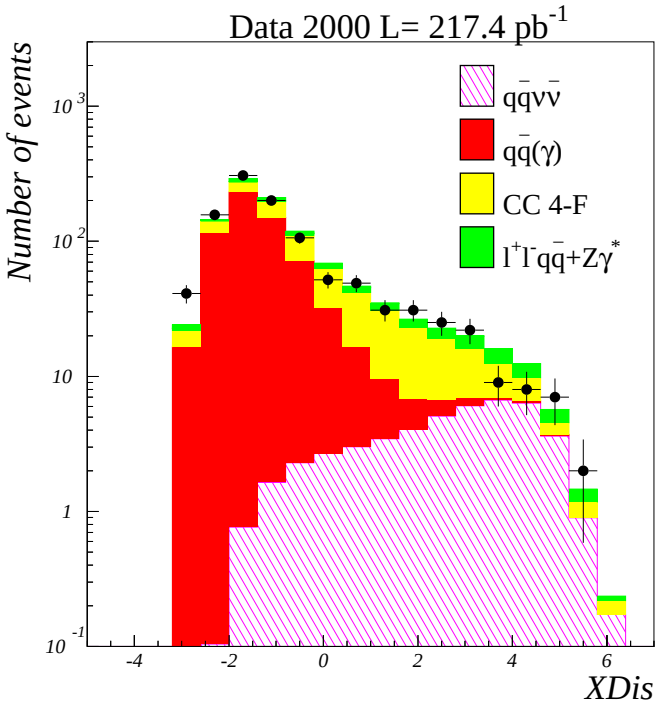

Figure 7: Combined discriminating variable for the $\nu\bar{\nu}q\bar{q}$ analysis (probabilistic selection) The dots are the data taken in 2000 at centre-of-mass energies $\sqrt{s}$ in the range 202-209 GeV. The histograms are the simulation prediction.

5.5 Results and comparison

The results from the two selections are presented in Table 4, where the observed and predicted numbers of events, selected after cuts on each discriminant variable maximising the product of the efficiency and purity, are shown[9]. As can be seen, the two methods gave compatible results, but the IDA selection was slightly more performant. There was an overall agreement between data and simulation within statistical errors in both cases. A study of the overlap between the two selections, performed with the data collected in 2000, showed that the proportion of common events was about 60% in real data: 55% in the background and 85% in the signal, according to the simulation. The IDA selection was used as the main analysis, and the probabilistic as cross-check.

At each centre-of-mass energy, a measurement of the production cross-section was obtained from a binned maximum likelihood fit to the distribution of the final IDA variable, with the ZZ signal contribution as the only free parameter. Cross-sections were also extracted from the probabilistic analysis, using the numbers of events and efficiences given in Table 4. The IDA selection was used to derive the combined values of the NC02 cross-section. The results obtained and the combinations performed with other channels are described in Section 10.

The residual background was composed of several processes. Near the threshold for

[9]The luminosities used to analyse the $ZZ \to \nu\bar{\nu}q\bar{q}$ channel were slightly lower than for other channels, because additional criteria on the operation of the apparatus were used.

$ZZ \to \nu\bar{\nu}q\bar{q}$ (IDA selection)					
$\sqrt{s}$ [GeV]	Integrated luminosity [pb^{-1}]	Selection efficiency	Predicted background	Predicted total MC	Selected data
183	52.4	0.31	1.6	3.1	2
189	152.8	0.49	14.8	28.3	22
192	24.9	0.56	5.1	8.1	6
196	75.0	0.52	13.3	22.6	27
200	82.2	0.56	18.7	31.0	25
202	40.4	0.48	7.5	13.0	12
205	72.9	0.54	16.8	27.9	22
207	138.4	0.52	30.7	51.9	49
Total	639.0	0.50	108.5	185.9	165
$ZZ \to \nu\bar{\nu}q\bar{q}$ (Probabilistic selection)					
$\sqrt{s}$ [GeV]	Integrated luminosity [pb^{-1}]	Selection efficiency	Predicted background	Predicted total MC	Selected data
189	152.8	0.46	24.3	36.7	32
192	24.9	0.50	5.6	8.5	9
196	75.0	0.46	12.7	21.4	20
200	82.2	0.46	16.4	26.0	25
202	40.4	0.51	10.9	16.6	16
205	72.9	0.48	18.0	28.4	24
207	138.4	0.45	29.6	47.6	48
Total	586.6	0.47	117.5	185.2	174

Table 4: Integrated luminosities, selection efficiencies and number of observed and expected events in the $ZZ \to \nu\bar{\nu}q\bar{q}$ channel, after cuts on the discriminant variable maximising the product of the efficiency and purity.

ZZ production, the main backgrounds were from $q\bar{q}(\gamma)$ events with badly reconstructed jets, and from WW processes. At higher energies, mis-reconstructed $q\bar{q}(\gamma)$ events were easier to suppress, thanks to the boost in the ZZ signal. In this case, the main background was from single-resonant $We\nu_e$ processes.

5.6 Systematic errors

The main sources of systematic error in the selection of $ZZ \to \nu\bar{\nu}q\bar{q}$ events were from uncertainties in the description of the energy flow reconstruction of the $q\bar{q}(\gamma)$ background and, to a lesser extent, from uncertainties in the predicted background cross-sections, particularly those of the single-resonant $We\nu_e$ process. The propagation of these uncertainties to the final steps of the IDA analysis was studied.

Large statistical samples of Z events, collected in the same conditions as the high energy data, were used to evaluate the errors in the energy flow reconstruction. The selection of $ZZ \to \nu\bar{\nu}q\bar{q}$ events exploits the large missing energy characteristic of this channel, and is hence sensitive to the description of the low energy tail in the reconstruction of background processes such as $q\bar{q}(\gamma)$. The collected Z events were compared to the simulation to estimate corrections to the particle flow, in several momentum bins, separately for the barrel and endcaps, and for charged and neutral particles. The corrections, consisting mainly of changes in multiplicities to account for observed efficiency losses and possible duplication effects in the pattern recognition, were typically only a few percent for charged particles, but could be larger in the case of neutral particles at low momentum or in the endcaps. It was found that the simulation overestimated particle reconstruction efficiencies in the highest momentum bins. This resulted in underestimating the lower tail of the total energy distribution. Application of the computed corrections significantly improved the overall agreement between data and simulation at pre-selection level, for all energy flow observables such as the total charged and neutral energies, the visible mass or the acoplanarity. Partial improvement also resulted in the tails of the distributions most relevant to the selection of $ZZ \to \nu\bar{\nu}q\bar{q}$ events, although comparisons were in this case limited by the statistics of the available samples.

This correction procedure was then applied to all simulated high energy samples, and the IDA analysis was repeated. The main effect was to increase the $q\bar{q}(\gamma)$ background in the high purity regions relevant to the signal extraction, by about one third on the average, while other components were much less affected. The ZZ cross-sections were then fitted using these modified versions of the simulation. The differences in expected results were used as conservative estimates of the errors representing the impact of the uncertainties in the energy reconstruction. Since these differences were always of the same sign, corresponding to reductions in the ZZ cross-section obtained, the specified errors were treated as one-sided. The magnitude of the effects was reduced above the ZZ production threshold, because of the decreasing relative importance of the $q\bar{q}(\gamma)$ background.

To reduce the overall uncertainty, regions where the $q\bar{q}(\gamma)$ background dominated were removed by a final cut on the discriminating variable, chosen to minimise the combined systematic and statistical error using the full LEP-2 data sample. The results are presented in Table 5. The combined effect from errors on predicted background cross-sections are also shown, assuming the following values [20]: $WW : \pm\ 2\%$, $We\nu : \pm\ 5\%$, $Z\gamma : \pm\ 2\%$. Both errors were assumed to be correlated between the energies analysed.

$\sqrt{s}$ [GeV]	Systematic error from energy flow	Systematic error from MC cross-sections
183	± 14.5 %	± 4.0 %
189	± 10.0 %	± 2.5 %
192	± 7.5 %	± 2.5 %
196 - 208	± 3.5 %	± 2.5 %

Table 5: Expected effects on the $ZZ \to \nu\bar{\nu}q\bar{q}$ cross-section fitted in the IDA analysis, from uncertainties in the energy flow reconstruction and predicted background cross-sections.

6 Jets and a pair of isolated muons or electrons

The $\mu^+\mu^- q\bar{q}$ and $e^+e^- q\bar{q}$ decay modes represent 9.3% of the ZZ final states. The two final state leptons are typically well isolated from all other particles. This can be used to select such events with high efficiency and low background contamination in both the muon and electron channels. Events were selected initially without explicit cuts on the masses of the final state fermion pairs, in order to analyse simultaneously the production of ZZ and $Z\gamma^*$ events and, in the case of the $e^+e^- q\bar{q}$ channel, contributions from single-resonant processes such as $(Z/\gamma^*)e^+e^-$. Mass cuts were then applied to isolate the ZZ contribution.

6.1 Selection procedure

A loose hadronic pre-selection was first applied, requiring that the events have at least 7 charged particles and a charged energy above 0.30 $\sqrt{s}$. To suppress the radiative return to the Z boson, events were rejected if a photon with energy more than 60 GeV was found. The selection procedures then proceeded in a closely similar way for both $\mu^+\mu^- q\bar{q}$ and $e^+e^- q\bar{q}$ channels. In order to maximize the lepton identification efficiency, any charged particle with a momentum exceeding 5 GeV/c was considered as a possible lepton candidate around which nearby photons, if present, could be clustered. This was found to be necessary to improve the energy evaluation in the presence of final state radiation, and, in the case of electrons, bremsstrahlung. In the case of the $e^+e^- q\bar{q}$ channel, photons with energy between 20 GeV and 60 GeV were also considered as electron candidates, to recover events in which the electron track was not reconstructed.

Events with at least two lepton candidates of the same flavour, opposite charge and invariant mass exceeding 2 GeV/c^2 were then selected. All particles except the lepton candidates were clustered into jets and a kinematic fit requiring four-momentum conservation was applied, correcting appropriately the errors on lepton energies in cases where photons had been added by the clustering procedure.

At least one of the two lepton candidates was required to satisfy strong lepton identification criteria, while softer requirements were specified for the second. Muons were considered as strongly identified if selected by the standard DELPHI muon identification package [11], based mainly on finding associated hits in the muon chambers. For soft muon identification only a set of kinematic and calorimetric criteria were used. Electrons were considered as strongly identified when the energy deposited in the electromagnetic calorimeter exceeded 60% of the cluster energy or 15 GeV and when the energy deposited

in the hadron calorimeter was limited. For soft electron identification only requirements on the momentum of the charged particle in the cluster and on the energy deposited in the hadron calorimeter were used. Moreover electron candidates originating from applying the clustering procedure around a photon were considered as softly identified.

Two discriminating variables were then used for final event selection: P_t^{min}, the lesser of the transverse momenta of the lepton candidates with respect to their nearest jet, and the χ^2 per degree of freedom of the kinematic fit.

6.2 Results

The distribution of the mass of one fermion pair ($M_{q\bar{q}}$ or $M_{\mu^+\mu^-,e^+e^-}$) when the mass of the second pair is within 15 GeV/c^2 of the nominal Z mass is shown in Figure 8a,b. The distribution of the sum of masses of two fermion pairs is shown in Figure 8c. The observed distributions are in reasonable agreement with the predictions from simulation. To select on-shell ZZ production, cuts were placed simultaneously on the masses of the l^+l^- pair, on the remaining hadron system and on their sum, taking into account in the performance optimization the different mass resolutions of these final states and the presence of the single-resonant process, e^+e^-Z in the case of the $e^+e^-q\bar{q}$ channel. The observed and predicted numbers of selected events are shown in Table 6. The residual background is composed of $l^+l^-q\bar{q}$ events generated outside the signal region, of other processes, principally W^+W^-, other ZZ decays and in the case of $e^+e^-q\bar{q}$, $q\bar{q}(\gamma)$ production. These results were used to derive the combined values of the NC02 cross-section described in Section 10.

6.3 Systematic errors

Several sources of systematic errors were investigated. Uncertainties in the lepton identification were estimated comparing semileptonic WW events selected in data and simulation using the strong lepton identification criteria. Uncertainties in signal efficiencies from the description of the kinematic observables used were evaluated comparing the P_t and χ^2 distributions in data and simulation for all $llq\bar{q}$ events selected without mass cuts. Corresponding uncertainties in background levels were evaluated by comparing samples of events selected in data and in simulation requiring both isolated tracks not to be identified as leptons, while maintaining all the other criteria. Finally, uncertainties in the background level in the $e^+e^-q\bar{q}$ channel from fake electrons were studied with $q\bar{q}(\gamma)$ events selected in data and in simulation with purely kinematic criteria. These effects and the statistical uncertainty of simulated data yielded a combined systematic error on the efficiency to select $\mu^+\mu^-q\bar{q}$ and $e^+e^-q\bar{q}$ events of $\pm$ 3.0%, and a relative uncertainty in the background level of $\pm$ 15%[10]. Finally, additional errors of 2% and 3% were added in the procedure to extract and combine the cross-sections with other channels (see Section 10), to account for uncertainties from the signal definition used (see Section 3), arising because of interference effects, and because of biases resulting from the single-resonant $(Z/\gamma^*)e^+e^-$ process, respectively. All systematic errors were assumed to be correlated between the energies analysed.

[10]In both cases determinations were limited in accuracy by the statistics of the available samples, and should be interpreted as upper bounds.

$ZZ \to \mu^+\mu^- q\bar{q}$					
$\sqrt{s}$ [GeV]	Integrated luminosity [pb^{-1}]	Selection efficiency	Predicted background	Predicted total MC	Selected data
183	54.0	0.88	0.04	0.52	3
189	158.1	0.87	0.22	4.14	5
192	25.8	0.89	0.05	0.91	0
196	76.9	0.88	0.12	2.71	1
200	84.3	0.87	0.15	3.20	5
202	41.1	0.84	0.08	1.62	0
205	83.3	0.87	0.17	3.34	2
207	141.8	0.84	0.30	5.70	5
Total	665.3	0.86	1.13	22.14	21
$ZZ \to e^+e^- q\bar{q}$					
$\sqrt{s}$ [GeV]	Integrated luminosity [pb^{-1}]	Selection efficiency	Predicted background	Predicted total MC	Selected data
183	54.0	0.72	0.18	0.73	0
189	158.1	0.74	0.64	4.19	3
192	25.8	0.75	0.13	0.93	1
196	76.9	0.74	0.36	2.73	4
200	84.3	0.74	0.45	3.27	2
202	41.1	0.72	0.17	1.50	1
205	83.3	0.74	0.34	3.30	4
207	141.8	0.70	0.55	5.37	4
Total	665.3	0.73	2.82	22.02	19

Table 6: Integrated luminosities, selection efficiencies and number of observed and expected selected events in the $ZZ \to \mu^+\mu^- q\bar{q}$ and $ZZ \to e^+e^- q\bar{q}$ channels.

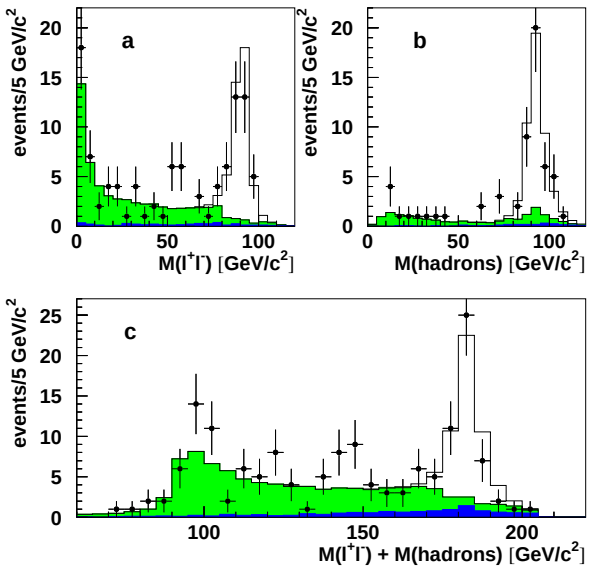

Figure 8: a) Distribution of the mass of the l^+l^- pair when the mass of the hadron system is within 15 GeV/c^2 of the nominal Z mass; b) Distribution of the mass of the hadron system when the mass of the l^+l^- pair is within 15 GeV/c^2 of the nominal Z mass; c) Distribution of the sum of the masses of the l^+l^- pair and of the hadron system. The dots are the data taken in 1997-2000 and the histograms represent the simulation. The contribution from the signal is indicated by the empty histogram. The contributions from backgrounds are indicated with light grey when arising from from $\mu^+\mu^- q\bar{q}$ or $e^+e^- q\bar{q}$ final states, and with dark filling otherwise.

7 Jets and a pair of isolated τ-leptons

The $\tau^+\tau^- q\bar{q}$ decay mode represents 4.7% of the ZZ final states. The search for $\tau^+\tau^- q\bar{q}$ final states was based on the inclusive selection of isolated clusters of particles with low charged multiplicity and low invariant mass. Each pair of such clusters was considered as a possible $\tau^+\tau^-$ candidate, with all other particles assumed to originate from a $q\bar{q}$ system. Assuming this topology, a set of discriminating variables reflecting the isolation of the clusters and the likelihood of the $\tau^+\tau^- q\bar{q}$ hypothesis was defined. All these variables were combined into a single one using a probabilistic method based on likelihood ratio products. Cutting on this combined variable enabled to select $\tau^+\tau^- q\bar{q}$ final states consistent with ZZ production with high efficiency and low background contamination.

7.1 Definition of τ-clusters

Each charged particle with momentum exceeding 1 GeV/c was considered as a τ-cluster candidate. Every other charged particle (with energy exceeding 1 GeV) and photon (with energy exceeding 0.5 GeV) was then successively added to each one of these candidates and the incremental change in the cluster mass ΔM_{cl} was computed. After sorting the particles in increasing order of ΔM_{cl}, that which produced the minimal ΔM_{cl} was kept if the charged and neutral particle cluster multiplicities were both less than 4, if ΔM_{cl} was less than 1.5 GeV/c^2 and, for clusters with one (more than one) charged particle, if their mass, M_{cl} was less than 2.5 (1.9) GeV/c^2.

After adding each particle, the determination of ΔM_{cl} was repeated for all remaining particles with the modified cluster. The procedure was continued until all combinations had been tried. If the initial charged particle was identified as an electron or a muon, only photons were added. To study the isolation of the so-defined τ-cluster candidates, the four-momenta of their tracks were subtracted from the jets to which they belonged, and the nearest jet with a remaining energy exceeding 3 (1.5) GeV, for a cluster with one (more than one) charged particle, was determined. Two variables characterising the isolation were defined: the angle θ_{cl} between the cluster and the nearest jet, and the transverse momentum P_t of the most energetic particle in the cluster with respect to the nearest jet.

7.2 Pre-selection

Events were required to have at least 7 charged particles and a charged energy greater than 0.30 $\sqrt{s}$. To suppress radiative returns to the Z, events were rejected if a photon with an energy exceeding 55% of the beam energy was found. At least two τ-clusters per event were required, satisfying the isolation criterion $|\cos\theta_{cl}| < 0.95$ (0.92), for clusters with one (more than one) charged particle, having a sum of charges $|Q_1 + Q_2| < 2$, and with at least one of these clusters containing only one charged particle.

All particles not used to define the two τ candidates were then clustered in jets and a kinematic fit [22] with six constraints, consisting of four momentum conservation and $M_{\tau^+\tau^-} = M_{q\bar{q}} = M_Z$, was applied to the event. To exploit the large missing energy in the τ decay, the missing energies of each τ-cluster, $D_E^{1,2}$ (defined as the differences between each fitted cluster energy, $E_{fit}^{1,2}$, and the corresponding measured value), were then required to satisfy:

- $\min(D_E^1, D_E^2) > -15$ GeV,
- $\min(D_E^1, D_E^2) > 10$ GeV if the clusters contained identified leptons of the same type,
- $D_E > 3$ GeV for τ-clusters containing an identified lepton,
- $D_E^1 + D_E^2 > 10$ GeV if one or both τ-clusters contained an identified lepton.

After all these pre-selection criteria, the total number of events selected in data and Monte Carlo were 505 and 460.7, respectively.

7.3 Probabilistic selection

A probabilistic method based on likelihood ratio products was used to combine several variables defined at the level of the τ-clusters ($E_{fit}^{1,2}$, $D_E^{1,2}$, $\cos\theta_{cl}^{1,2}$, $P_t^{1,2}$), and the χ^2 probabilities of three kinematic fits, performed using exclusively the constraints from four-momentum conservation, using in addition the hypothesis of ZZ production (as described in section 7.2), or that of WW production (requiring the two di-jet masses reconstructed in the pairing with smallest χ^2 to be equal to M_W). The probability density functions were determined for each quantity by combining the predictions from all centre-of-mass energies, separately for τ-clusters with leptons, with one charged particle and with more than one charged particle. The separation power of Y, the combined discriminant variable obtained, is illustrated in Figure 9, where the distribution of $-\log_{10} Y$ is shown for a sample enriched with signal events by requiring $M_{\tau^+\tau^-}$ and $M_{q\bar{q}}$ to be compatible with the Z boson mass.

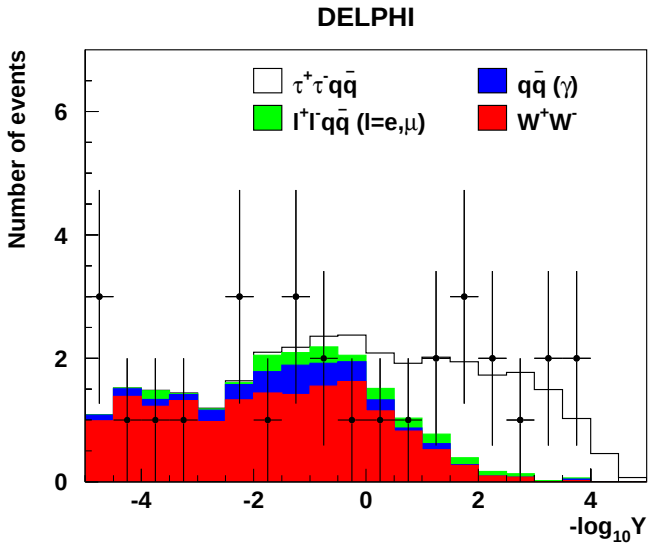

Figure 9: Combined discriminating variable for the $\tau^+\tau^- q\bar{q}$ analysis, obtained after enriching with signal events by requiring $M_{\tau^+\tau^-}$ and $M_{q\bar{q}}$ to be compatible with the Z boson mass. The dots are the data taken in 1997-2000 and the histograms represent the simulation.

7.4 Results

To isolate the on-shell ZZ production process, a cut, chosen to maximise the product of the efficiency and purity, was applied on the combined variable: $-\log_{10} Y > 0.5$. The fermion pair mass distributions for the events selected by this cut ($M_{\tau^+\tau^-}$ and $M_{q\bar{q}}$) are shown in Figure 10, obtained through kinematic fitting of the event with the constraints from four-momentum conservation only. The observed distributions are in reasonable agreement with the predictions from simulation. For final selection, additional cuts were placed on these two masses, and on their sum, in order to further improve the signal

to background ratio. The observed and predicted numbers of selected events are shown in Table 7. The background is composed of $q\bar{q}q\bar{q}$, $l^+l^-q\bar{q}$ and $q\bar{q}(\gamma)$ events. The $q\bar{q}q\bar{q}$ final states were primarily from WW decays. The overall contribution from other ZZ decays was less than 30% of the total background. These results were used to derive the combined values of the NC02 cross-section described in Section 10.

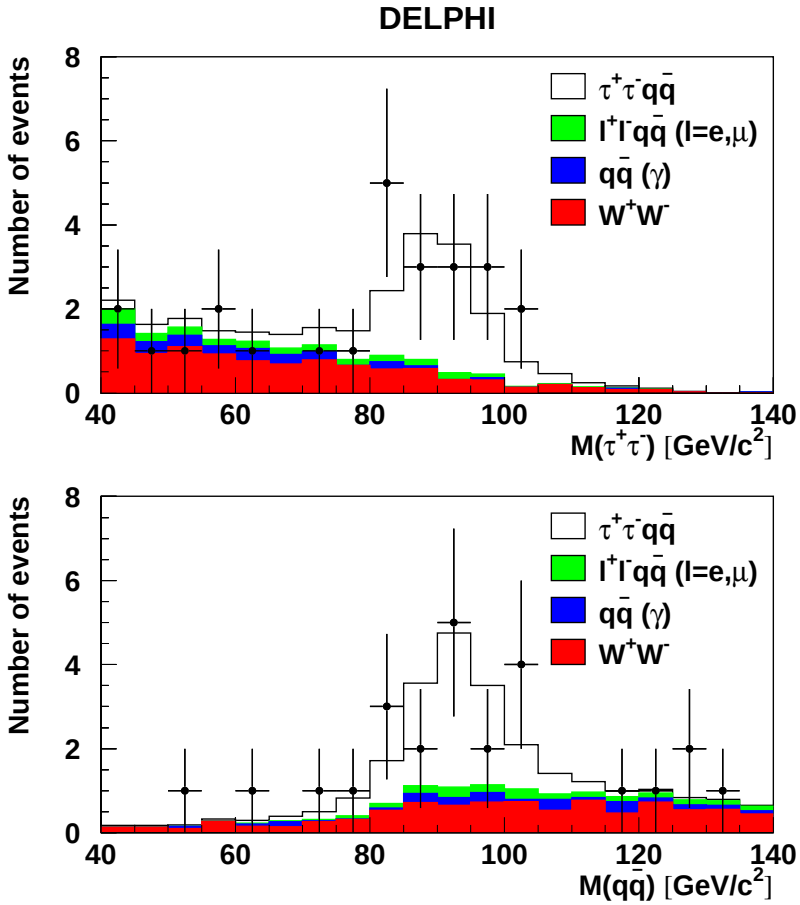

Figure 10: Distribution of $M_{\tau^+\tau^-}$ and $M_{q\bar{q}}$, obtained through kinematic fitting of the event with the constraints from four-momentum conservation only, for the selected events. The dots are the data taken in 1997-2000 and the histograms represent the simulation.

7.5 Systematic errors

The main source of systematic error in the selection of $ZZ \to \tau^+\tau^-q\bar{q}$ events were from uncertainties in the reconstruction of the τ-clusters and associated isolation variables. After the pre-selection, about $\pm$ 10% more events were selected in data as compared to Monte Carlo (see Section 7.2). This discrepancy was used to represent the systematic uncertainty in the selection efficiency. Moreover, the fraction of background events originating from other ZZ decays (see Section 7.4) was neglected in the procedure to derive combined NC02 cross-sections. A $\pm$ 30% uncertainty in the background level was assigned

$ZZ \to \tau^+\tau^- q\bar{q}$					
$\sqrt{s}$ [GeV]	Integrated luminosity [pb^{-1}]	Selection efficiency	Predicted background	Predicted total MC	Selected data
183	54.0	0.28	0.09	0.28	0
189	158.1	0.34	0.52	2.08	1
192	25.8	0.40	0.12	0.49	0
196	76.9	0.41	0.32	1.56	0
200	84.3	0.41	0.42	1.91	1
202	41.1	0.41	0.20	0.94	2
205	83.3	0.41	0.38	1.91	4
207	141.8	0.40	0.64	3.26	5
Total	665.3	0.38	2.69	12.43	13

Table 7: Integrated luminosities, selection efficiencies and number of observed and expected selected events in the $ZZ \to \tau^+\tau^- q\bar{q}$ channel, after cuts on $M_{\tau^+\tau^-}$, $M_{q\bar{q}}$ and on their sum.

to cover this effect. Both errors were assumed to be correlated between the centre-of-mass energies analysed.

8 Four-lepton final states

The $l^+l^-l^+l^-$ decay mode represents 1.0% of the ZZ final states. The event topology is clean and the only significant background comes from non-resonant $e^+e^-l^+l^-$ production.

8.1 Selection procedure

Events were first selected if they contained between 4 and 8 charged particles, accompanied by at most 10 neutral particles, irrespective of particle identification. In order to take into account final state radiation and bremsstrahlung effects for candidate electrons, the momenta of the charged particles were rescaled if the measured sum of energies of electromagnetic clusters in a narrow cone around the track direction was larger than the energy inferred from the track momentum measurement. The total invariant mass of the charged particles had to be greater than 50 GeV/c^2, and the minimum invariant mass after discarding any one of the charged particles larger than 20 GeV/c^2. All combinations of four charged particles with total charge zero were then examined, and a combination was selected if:

- all four tracks had their impact parameters at the interaction point smaller than 3.0 and 0.5 cm, respectively in the projections containing the beam axis and perpendicular to it, and polar angles between 10° and 170°,
- at least three of the four charged particles had momenta greater than 5 GeV/c, and the least energetic particle a momentum greater than 2 GeV/c,

- a system of two oppositely charged particles was found with both their invariant and recoil masses within 10 GeV/c^2 of the Z boson mass and having the same flavour (when both were identified as either electrons or muons),
- the two particles complementary to this system were separated by at least 90° from each other,
- the invariant mass of all pairs of oppositely charged particles in the event exceeded 5 GeV/c^2.

8.2 Results

The observed and predicted numbers of selected events are shown in Table 8. They are in overall agreement within the statistical errors. These results were used to derive the combined values of the NC02 cross-section described in Section 10. The two events selected at $\sqrt{s} = 188.6$ and 199.5 GeV were in the $\mu^+\mu^-e^+e^-$ and $\mu^+\mu^-\mu^+\mu^-$ final states, respectively. An event display for the latter is shown in Figure 11.

$ZZ \to l^+l^-l^+l^-$					
$\sqrt{s}$ [GeV]	Integrated luminosity [pb^{-1}]	Selection efficiency	Predicted background	Predicted total MC	Selected data
183	54.0	0.53	0.09	0.17	0
189	158.1	0.62	0.15	0.76	1
192	25.8	0.58	0.06	0.19	0
196	76.9	0.54	0.13	0.47	0
200	84.3	0.54	0.17	0.60	1
202	41.1	0.54	0.07	0.27	0
205	83.3	0.50	0.22	0.62	0
207	141.8	0.41	0.28	0.84	0
Total	665.3	0.53	1.17	3.92	2

Table 8: Integrated luminosities, selection efficiencies and number of observed and expected selected events in the $ZZ \to l^+l^-l^+l^-$ channel.

8.3 Systematic errors

The main sources of systematic error in the analysis of the $ZZ \to l^+l^-l^+l^-$ channel were from limited statistics in the Monte Carlo samples used to compute the residual background and the selection efficiency, and from approximations used in the interpretion of the results in terms of the NC02 cross-section. These three uncertainties amounted to ± 12%, ± 5% and ± 5%, respectively. The latter was assumed to be correlated between the energies analysed. These errors dominated over uncertainties in background cross-sections and reconstruction.

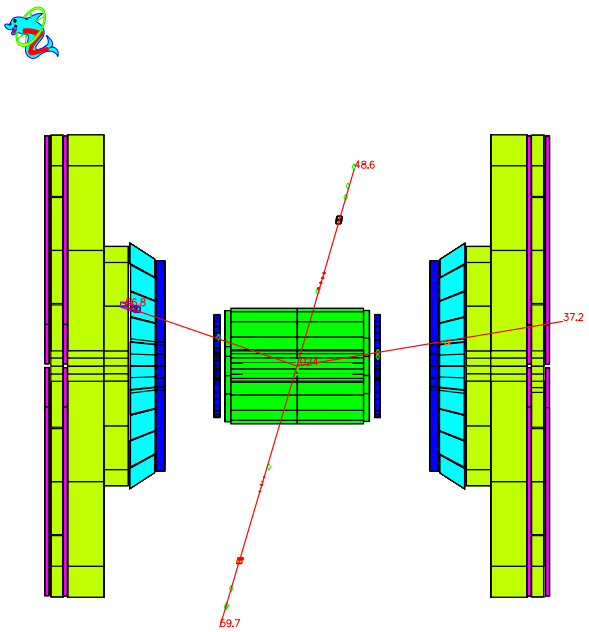

Figure 11: The ZZ $\rightarrow \mu^+\mu^-\mu^+\mu^-$ candidate selected at 199.5 GeV centre-of-mass energy. Three muons are observed in the barrel and one in the forward part of the detector. A kinematic fit was performed assuming the production of two identical heavy objects, each decaying into $\mu^+\mu^-$. Out of two possible combinations to form the $\mu^+\mu^-$ pairs the highest probability was found for the top-bottom and left-right pairs. The measured invariant mass of the object, 90.8 GeV/c^2, is fully compatible with ZZ production.

9 Two isolated leptons with missing energy

The $\nu\bar{\nu}\mu^+\mu^-$ and $\nu\bar{\nu}e^+e^-$ decay modes represent 2.7% of the ZZ final states. The events are characterized by two acollinear charged leptons of the same flavour, with both invariant and recoil masses close to the Z mass, and by large missing energy. Although it has different production kinematics, the WW process also contributes to these final states with a large cross-section. A significant fraction of the corresponding events have exactly the same features and constitute a dominant background.

9.1 Selection procedure

To ensure good reconstruction, tracks were required to have impact parameters at the interaction point smaller than 3.0 and 0.5 cm, respectively in the projections containing the beam axis and perpendicular to it, and polar angles between 20° and 160°. Final state radiation and bremsstrahlung effects for candidate electrons were taken into account as discussed in Section 8.1 for the four-lepton analysis. Events with two particles identified as e^+e^- or $\mu^+\mu^-$ were selected if their total energy was less than 60% of that of the centre-of-mass, if the angle between them was in the range $[\theta_{min}$,170°], where θ_{min} =

$0.95 \arccos(1 - 8m_Z^2/s)$, if the polar angle of the missing momentum vector was between 25° and 155°, and if the reconstructed invariant masses satisfied:

- $\min\{\mid M_Z - m(l^+l^-) \mid , \mid M_Z - m_{recoil}(l^+l^-) \mid\} < 4$ GeV/c^2,
- $\max\{\mid M_Z - m(l^+l^-) \mid , \mid M_Z - m_{recoil}(l^+l^-) \mid\} < 8$ GeV/c^2,

where $m_{recoil}(l^+l^-)$ is the invariant mass recoiling against the l^+l^- pair.

9.2 Results

The observed and predicted numbers of selected events are shown in Table 9. They are in reasonable overall agreement, within the statistics. These results were used to derive the combined values of the NC02 cross-section described in Section 10.

$ZZ \to \nu\bar{\nu}\mu^+\mu^-, \nu\bar{\nu}e^+e^-$					
$\sqrt{s}$ [GeV]	Integrated luminosity [pb^{-1}]	Selection efficiency	Predicted background	Predicted total MC	Selected data
183	54.0	0.30	0.31	0.42	0
189	158.1	0.32	0.80	1.65	2
192	25.8	0.35	0.16	0.34	2
196	76.9	0.33	0.74	1.32	2
200	84.3	0.32	0.72	1.39	1
202	41.1	0.29	0.36	0.68	0
205	83.3	0.27	0.58	1.18	1
207	141.8	0.25	1.00	1.94	2
Total	665.3	0.30	4.67	8.92	10

Table 9: Integrated luminosities, selection efficiencies and number of observed and expected selected events in the $ZZ \to \nu\bar{\nu}\mu^+\mu^-, \nu\bar{\nu}e^+e^-$ channels.

9.3 Systematic errors

The main sources of systematic error in the analysis of the $ZZ \to \nu\bar{\nu}\mu^+\mu^-, \nu\bar{\nu}e^+e^-$ channels were from limited statistics in the Monte Carlo samples used to compute the residual background and the selection efficiency, and from uncertainties in the background level. These uncertainties, amounted to ± 13%, ± 5% and ± 5%, respectively, and dominated over errors on the selection efficiency or uncertainties from the approximations used in the interpretion of the results in terms of the NC02 cross-section. The uncertainty in the background level was assumed to be correlated between the energies analysed.

10 Combined NC02 cross-sections

The measurements described in the previous sections for the different ZZ sub-channels showed a reasonable general agreement between the data and simulation. In this section

the comparison is presented more globally, in terms of extracted NC02 cross-sections combined over all channels at each centre-of-mass energy, as well as over all energies (by normalising to the SM predictions), both separately in each sub-channel, and for all channels together. Such combinations enabled more comprehensive and statistically meaningful checks of the SM prediction. Cross-sections for individual sub-channels are also given at each energy in the case of the most important ZZ final states.

10.1 Likelihood method

To obtain the cross-section information in the different cases, the probability functions at each energy and for each sub-channel, defined with respect to variations of the value of the NC02 cross-section, were combined into global likelihoods. For the channels $q\bar{q}q\bar{q}$ and $\nu\bar{\nu}q\bar{q}$ (analysed in the IDA stream), the shapes of the probability functions were derived from the fits to the distributions of the combined variables defined in each of the corresponding analyses. For the remaining channels the Poissonian probabilities were constructed, based on the numbers of events selected in the data and predicted in the simulation as background. The central value for each measurement was defined as the median of the corresponding likelihood. The statistical errors were obtained from the interval around the median which contained 68.26% of the probability. In cases when less than 31.74% of the probability was below the maximum of the likelihood, an upper limit was given, defined as the value for which 95% of the probability was below.

10.2 Propagation of systematic errors

The propagation of systematic uncertainties affecting each different final state to its probability function was studied by introducing appropriately modified assumptions for backgrounds and efficiencies (as described in the corresponding sections). Moreover channel-correlated uncertainties on the integrated luminosities collected at each centre-of-mass energy point were also taken into account. They amounted to 0.6% (theory error) and 0.3% (measurement error) and were respectively correlated and uncorrelated among the energies.

The following procedure was applied to propagate all systematic errors in the combination of any selection of channels or energy points. Uncertainties were divided into four groups according to their correlation among energies and channels. Gaussian random numbers were then drawn and assigned taking into account the nature of the error (common random number among channels or energies in cases of correlated errors, and independent ones otherwise). The probability functions were then modified accordingly and their combination was repeated a large number of times. The standard deviation of the Gaussian-like distribution of central values obtained was taken to represent the total systematic error affecting the combined measurement for the selection of channels or energy points considered.

10.3 Results

The measured values of the NC02 cross-sections at each centre-of-mass energy are listed in Table 10 and shown in Figure 12, together with the SM predictions from the YFSZZ

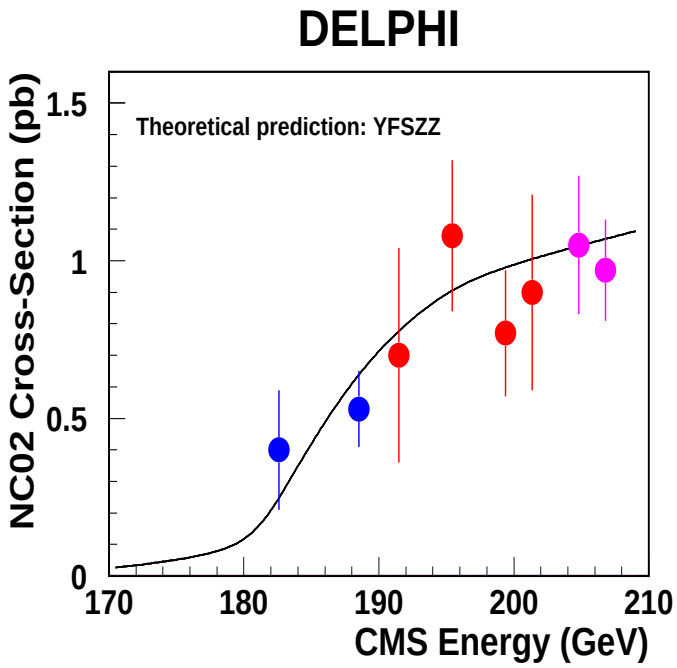

Figure 12: Combined NC02 cross-sections measured from data collected in 1997-2000. The solid curve was computed using the YFSZZ Monte-Carlo [27]. Values obtained with the EXCALIBUR Monte-Carlo were within ±1% of those obtained with YFSZZ.

generator [27]. These measurements, normalised to the predicted SM values, were also combined into a single value:

$$\mathrm{R_{NC02}} = 0.91 \pm 0.08\ (stat) \pm 0.02\ (syst)$$

Both the combined result and the values at the different energies show a good global agreement with the SM predictions, at the level of one standard deviation. The expected weights of each measurement in the combination are given in Table 10.

The combination of the results from the different energies was also performed for each sub-channel separately. The results are listed in Table 11, with the expected weight of each channel in the global combination described above, and with the corresponding ZZ branching fraction. They are also shown graphically in Figure 13. The channels were ordered according to their expected weight. This order was not always correlated to the decay branching ratios because of the different background conditions. As can be seen, the three main channels $ZZ \to q\bar{q}q\bar{q}, \nu\bar{\nu}q\bar{q}$ and $l^+l^-q\bar{q}$ (with $l = e, \mu$) had similar weights, and accounted for over 90% of the total sensitivity. A fair overall agreement with the SM predictions can be observed. The results in the two $\nu\bar{\nu}q\bar{q}$ analysis streams (IDA and Probabilistic) were compatible. This channel had the largest systematic uncertainty of all (relative to statistical errors). However, in this channel as in all others, systematic uncertainties were much smaller than the statistical errors. In the four-lepton channel, only an 95% CL upper limit could be quoted. The χ^2 of the seven measurements (excluding the $\nu\bar{\nu}q\bar{q}$ cross-check analysis) had a probability of 70%.

$\sqrt{s}$ [GeV]	σ_{NC02} [pb]	SM prediction [pb]	Expected weight [%]
183	$0.40^{+0.21}_{-0.16} \pm 0.02$	0.25	1.8
189	$0.53^{+0.12}_{-0.11} \pm 0.02$	0.65	17.4
192	$0.70^{+0.37}_{-0.31} \pm 0.02$	0.78	3.6
196	$1.08^{+0.25}_{-0.22} \pm 0.02$	0.90	12.7
200	$0.77^{+0.21}_{-0.18} \pm 0.02$	0.99	15.1
202	$0.90^{+0.33}_{-0.29} \pm 0.02$	1.00	7.3
205	$1.05^{+0.23}_{-0.20} \pm 0.02$	1.05	14.8
207	$0.97^{+0.16}_{-0.15} \pm 0.02$	1.07	27.3

Table 10: Measured and predicted NC02 cross-sections at the different energy points. The last column contains the expected weight of each energy point in the global combination performed over all energies.

$\sqrt{s}$ [GeV]	R_{NC02}	Expected weight [%]	Branching Fraction [%]
$q\bar{q}q\bar{q}$	$1.05^{+0.14}_{-0.14} \pm 0.04$	37.3	48.9
$\nu\bar{\nu}q\bar{q}$	$0.78^{+0.15}_{-0.15} \pm 0.05$	24.2	28.0
$\mu^+\mu^- q\bar{q}$	$0.93^{+0.22}_{-0.20} \pm 0.03$	15.6	4.6
$e^+e^- q\bar{q}$	$0.78^{+0.22}_{-0.19} \pm 0.03$	14.3	4.6
$\tau^+\tau^- q\bar{q}$	$1.12^{+0.40}_{-0.34} \pm 0.12$	5.5	4.6
$l^+l^-l^+l^-$	< 1.88	1.6	1.0
$\nu\bar{\nu}l^+l^-$	$1.52^{+0.86}_{-0.70} \pm 0.11$	1.5	2.7
$\nu\bar{\nu}q\bar{q}$ (Cross-check)	$0.80^{+0.19}_{-0.18}$	-	28.0

Table 11: Ratios of measured to predicted cross-sections for individual channels combined over all energy points. The two last columns contains the weight of the channel in the global combination over all channels described in the text, and the corresponding ZZ branching fraction.

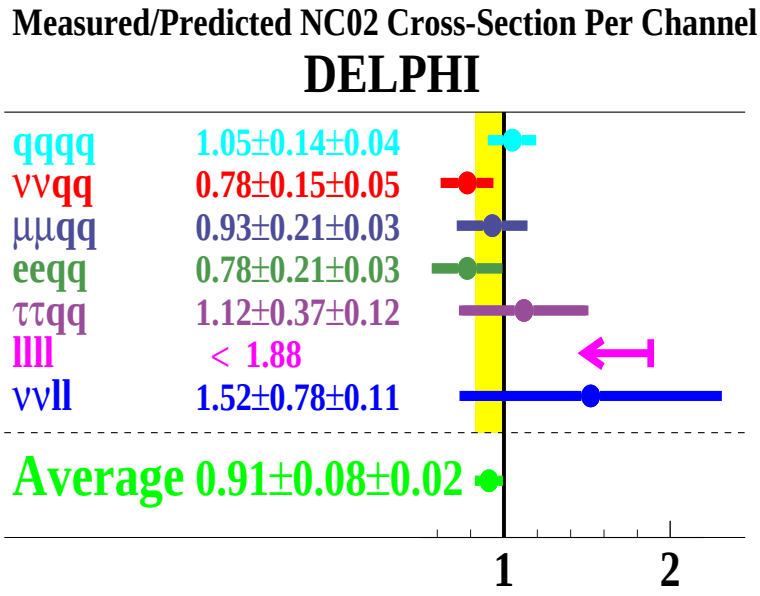

Figure 13: Ratios of measured to predicted cross-sections for individual channels combined over all energy points. The vertical band displays the total error on the combination of the seven channels.

Finally, for completeness, the values of the measured cross-sections normalised to the SM predictions are also presented at each energy in Table 12 for the three dominant channels.

Acknowledgements

We are greatly indebted to our technical collaborators, to the members of the CERN-SL Division for the excellent performance of the LEP collider, and to the funding agencies for their support in building and operating the DELPHI detector.

References

[1] Proceedings of the 29$^{\text{th}}$ International Conference on High Energy Physics, Vancouver, B.C., Canada, July 23-29 1998, eds. A.Astbury, D.Axen, J.Robinson, World Scientific 1999, talk by Michael Kobel, *Single and Pair Production of Neutral Electroweak Gauge Bosons*, page 454.

[2] DELPHI Collaboration, P.Aarnio *et al.*, Nucl. Instr. and Meth. **A303** (1991) 233.

[3] D. Chang, W-Y Keung and P.B. Pal, Phys. Rev. **D51** (1995) 1326.

$\sqrt{s}$ [GeV]	$q\bar{q}q\bar{q}$	$\nu\bar{\nu}q\bar{q}$	$\nu\bar{\nu}q\bar{q}$ (Cross-check)	$l^+l^-q\bar{q}$ ($l = e, \mu$)
183	< 4.21	< 3.72	-	$3.49^{+2.15}_{-1.54}$
189	$1.03^{+0.39}_{-0.33}$	$0.59^{+0.34}_{-0.28}$	$0.63^{+0.42}_{-0.35}$	$0.98^{+0.41}_{-0.32}$
192	$1.34^{+0.84}_{-0.67}$	< 2.27	$1.49^{+1.17}_{-0.88}$	< 2.83
196	$1.71^{+0.52}_{-0.47}$	$1.36^{+0.54}_{-0.45}$	$0.90^{+0.54}_{-0.45}$	$0.93^{+0.51}_{-0.37}$
200	$0.78^{+0.35}_{-0.28}$	$0.63^{+0.41}_{-0.34}$	$0.88^{+0.50}_{-0.43}$	$1.10^{+0.48}_{-0.37}$
202	$1.12^{+0.55}_{-0.45}$	$1.31^{+0.82}_{-0.64}$	$1.01^{+0.73}_{-0.58}$	< 1.41
205	$1.17^{+0.37}_{-0.32}$	$0.68^{+0.42}_{-0.34}$	$0.65^{+0.48}_{-0.38}$	$0.90^{+0.42}_{-0.33}$
207	$1.02^{+0.25}_{-0.22}$	$0.91^{+0.34}_{-0.29}$	$1.02^{+0.38}_{-0.35}$	$0.78^{+0.31}_{-0.24}$

Table 12: Measured cross-sections normalised to the SM predictions for individual channels at individual centre-of-mass energies.

[4] K. Agashe, N.G. Deshpande, Phys. Lett. **B456** (1999) 60.

[5] K. Hagiwara, R.D. Peccei, D. Zeppenfeld and K. Hikasa, Nucl. Phys. **B282** (1987) 253.

[6] DELPHI collaboration, P.Abreu *et al.*, Phys. Lett. **B499** (2001) 23.
DELPHI collaboration, J.Abdallah *et al.*, Eur. Phys. J. **C23** (2002) 409.

[7] DELPHI Collaboration, P. Abreu *et al.*, Phys. Lett. **B497** (2001) 199.

[8] ALEPH Collaboration, R. Barate *et al.*, Phys. Lett. **B469** (1999) 287.

[9] L3 Collaboration, M. Acciarri *et al.*, Phys. Lett. **B465** (1999) 363.
L3 Collaboration, M. Acciarri *et al.*, Phys. Lett. **B497** (2001) 23.

[10] OPAL Collaboration, G. Abbiendi *et al.*, Phys. Lett. **B476** (2000) 256.

[11] DELPHI Collaboration, P.Abreu *et al.*, Nucl. Instr. and Meth. **A378** (1996) 57.

[12] V. Chabaud *et al.*, Nucl. Instr. and Meth. **A368** (1996) 314.

[13] F.A. Berends, R. Pittau, and R. Kleiss, Comp. Phys. Comm. **85** (1995) 437; see also *Physics at LEP2* G. Altarelli, T. Sjöstrand and F. Zwirner (eds.) CERN 96-01 (1996) Vol. 2, 23.

[14] T. Sjöstrand, Comp. Phys. Comm. **39** (1986) 347; T. Sjöstrand, `PYTHIA 5.6` *and* `JETSET 7.3`, CERN-TH/6488-92; see also *Physics at LEP2* G. Altarelli, T. Sjöstrand and F. Zwirner (eds.) CERN 96-01 (1996) Vol. 2, 41.

[15] Y. Kurihara *et al.*, in *Physics at LEP2* G. Altarelli, T. Sjöstrand and F. Zwirner (eds.) CERN 96-01 (1996) Vol. 2, 30.

[16] S. Jadach, B.F.L. Ward, Z. Was, Comp. Phys Comm. **124** (2000) 233; see also S. Jadach, B.F.L. Ward, Z. Was, Comp. Phys Comm. **79** (1994) 503.

[17] S. Jadach, W. Placzek, B.F.L. Ward, Phys. Lett **B390** (1997) 298.

[18] T. Alderweireld *et al.*, CERN-OPEN-2000-141.

[19] F. A. Berends, P. H. Daverveldt, R. Kleiss, Comp. Phys. Comm. **40** (1986) 271-284, 285-307, 309.

[20] E. Accomando *et al.*, *Four-fermion production in electron-positron collisions*, Reports of the working groups on precision calculations for LEP2 Physics, S. Jadach, G. Passarino, R. Pittau (eds.) CERN 2000-009 (2000), 1.

[21] G.Borisov, Nucl. Instr. Meth. **A417** (1998), 384

[22] see section 5.2 in DELPHI Collaboration, P. Abreu *et al.*, Eur. Phys. J. **C2** (1998) 581.

[23] A. Ballestrero *et al.*, *Report of the QCD Working Group*, Reports of the working groups on precision calculations for LEP2 Physics, S. Jadach, G. Passarino, R. Pittau (eds.) CERN 2000-009 (2000), 137.

[24] DELPHI Collaboration, P. Abreu *et al.*, Z. Phys. **C73** (1996) 11.

[25] DELPHI Collaboration, P. Abreu *et al.*, Eur. Phys. J. **C10** (1999) 415.

[26] T.G.M. Malmgren, Comp. Phys. Comm. **106** (1997) 230;
T.G.M. Malmgren and K.E. Johansson, Nucl. Inst. Meth. **403** (1998) 481.

[27] S. Jadach, W. Placzek, B.F.L. Ward, Phys. Rev. **D56** (1997) 6939.